Chapter 22

Discrete symmetries

Utility of discrete symmetries in reducing spectrum calculations is familiar from quantum mechanics. Here we show that the classical spectral determinants factor in essentially the same way as in quantum mechanics. In the process we also learn how to simplify the classical dynamics. The main result of this chapter can be stated as follows:

If the dynamics possesses a discrete symmetry, the contribution of a cycle p of multiplicity m_p to a dynamical zeta function factorizes into a product over the d_α-dimensional irreducible representations D_α of the symmetry group,

$$(1-t_p)^{m_p} = \prod_\alpha \det\,(1-D_\alpha(h_{\tilde p})t_{\tilde p})^{d_\alpha}\,, \quad t_p = t_{\tilde p}^{\,g/m_p}\,,$$

where $t_{\tilde p}$ is the cycle weight evaluated on the fundamental domain, g is the dimension of the group, $h_{\tilde p}$ is the group element relating the fundamental domain cycle $\tilde p$ to a segment of the full space cycle p, and m_p is the multiplicity of the p cycle. As the dynamical zeta functions have particularly simple cycle expansions, a simple geometrical shadowing interpretation of their convergence, and as they suffice for determination of leading eigenvalues, we shall concentrate in this chapter on their factorizations; the full spectral determinants can be factorized by the same techniques. To emphasize the group theoretic structure of zeta functions, we shall combine all the non-group-theory dependence of a p-cycle into a cycle weight t_p.

This chapter is meant to serve as a detailed guide to computation of dynamical zeta functions and spectral determinants for systems with discrete symmetries. Familiarity with basic group-theoretic notions is assumed, with the definitions relegated to appendix H.1. We develop here the cycle expansions for factorized determinants, and exemplify them by working out a series of cases of physical interest: C_2, C_{3v} symmetries in this chapter, and C_{2v}, C_{4v} symmetries in appendix H below.

22.1 Preview

Dynamical systems often come equipped with discrete symmetries, such as the reflection and the rotation symmetries of various potentials. Such symmetries simplify and improve the cycle expansions in a rather beautiful way; they can be exploited to relate classes of periodic orbits and reduce dynamics to a fundamental domain. Furthermore, in classical dynamics, just as in quantum mechanics, the symmetrized subspaces can be probed by linear operators of different symmetries. If a linear operator commutes with the symmetry, it can be block-diagonalized, and, as we shall now show, the associated spectral determinants and dynamical zeta functions factorize.

Invariance of a system under symmetries means that the symmetry image of a cycle is again a cycle, with the same weight. The new orbit may be topologically distinct (in which case it contributes to the multiplicity of the cycle) or it may be the same cycle, shifted in time. A cycle is *symmetric* if some symmetry operations act on it like a shift in time, advancing the starting point to the starting point of a symmetry related segment. A symmetric cycle can thus be subdivided into a sequence of repeats of an *irreducible segment*. The period or any average evaluated along the full orbit is given by the sum over the segments, whereas the stability is given by the product of the stability matrices of the individual segments.

Cycle degeneracies induced by the symmetry are removed by *desymmetrization*, reduction of the full dynamics to the dynamics on a *fundamental domain*. The state space can be completely tiled by a fundamental domain and its symmetry images. The irreducible segments of cycles in the full space, folded back into the fundamental domain, are closed orbits in the reduced space.

22.1.1 3-disk game of pinball

We have already exploited a discrete symmetry in our introduction to the 3-disk game of pinball, sect. 1.3. As the three disks are equidistantly spaced, our game of pinball has a sixfold symmetry. The symmetry group of relabeling the 3 disks is the permutation group S_3; however, it is better to think of this group geometrically, as C_{3v}, the group of rotations by $\pm 2\pi/3$ and reflections across the three symmetry axes. Applying an element (identity, rotation by $\pm 2\pi/3$, or one of the three possible reflections) of this symmetry group to any trajectory yields another trajectory. For instance, the cycles $\overline{12}$, $\overline{23}$, and $\overline{13}$, are related to each other by rotation by $\pm 2\pi/3$, or, equivalently, by a relabeling of the disks.

An irreducible segment corresponds to a periodic orbit in the *fundamental domain*, a one-sixth slice of the full 3-disk system, with the symmetry axes acting as reflecting mirrors, see figure 11.6. A set of orbits related in the full space by discrete symmetries maps onto a single fundamental domain orbit. The reduction to the fundamental domain desymmetrizes the

dynamics and removes all global discrete symmetry induced degeneracies: rotationally symmetric global orbits (such as the 3-cycles $\overline{123}$ and $\overline{132}$) have degeneracy 2, reflection symmetric ones (such as the 2-cycles $\overline{12}$, $\overline{13}$ and $\overline{23}$) have degeneracy 3, and global orbits with no symmetry are 6-fold degenerate. Table 11.2 lists some of the shortest binary symbols strings, together with the corresponding full 3-disk symbol sequences and orbit symmetries. Some examples of such orbits are shown in figure 22.3.

We shall return to the 3-disk game of pinball desymmetrization in sects. 22.2.2 and 22.6, but first we develop a feeling for discrete symmetries by working out a simple 1-d example.

22.1.2 Reflection symmetric 1-d maps

Consider f, a map on the interval with reflection symmetry $f(-x) = -f(x)$. A simple example is the piecewise-linear sawtooth map of figure 22.1.

Denote the reflection operation by $\mathbf{C}x = -x$. The symmetry of the map implies that if $\{x_n\}$ is a trajectory, than also $\{\mathbf{C}x_n\}$ is a trajectory because $\mathbf{C}x_{n+1} = \mathbf{C}f(x_n) = f(\mathbf{C}x_n)$. The dynamics can be restricted to a fundamental domain, in this case to one half of the original interval; every time a trajectory leaves this interval, it can be mapped back using $\mathbf{C}$. Furthermore, the evolution operator commutes with $\mathbf{C}$, $\mathcal{L}(y,x) = \mathcal{L}(\mathbf{C}y, \mathbf{C}x)$. $\mathbf{C}$ satisfies $\mathbf{C}^2 = \mathbf{e}$ and can be used to decompose the state space into mutually orthogonal symmetric and antisymmetric subspaces by means of projection operators

$$\begin{aligned} P_{A_1} &= \frac{1}{2}(\mathbf{e}+\mathbf{C})\,, \qquad P_{A_2} = \frac{1}{2}(\mathbf{e}-\mathbf{C})\,, \\ \mathcal{L}_{A_1}(y,x) &= P_{A_1}\mathcal{L}(y,x) = \frac{1}{2}\left(\mathcal{L}(y,x)+\mathcal{L}(-y,x)\right)\,, \\ \mathcal{L}_{A_2}(y,x) &= P_{A_2}\mathcal{L}(y,x) = \frac{1}{2}\left(\mathcal{L}(y,x)-\mathcal{L}(-y,x)\right)\,. \end{aligned} \tag{22.1}$$

To compute the traces of the symmetrization and antisymmetrization projection operators (22.1), we have to distinguish three kinds of cycles: asymmetric cycles a, symmetric cycles s built by repeats of irreducible segments $\tilde{s}$, and boundary cycles b. Now we show that the spectral determinant can be written as the product over the three kinds of cycles: $\det(1-\mathcal{L}) = \det(1-\mathcal{L})_a \det(1-\mathcal{L})_{\tilde{s}} \det(1-\mathcal{L})_b$.

Asymmetric cycles: A periodic orbits is not symmetric if $\{x_a\} \cap \{\mathbf{C}x_a\} = \emptyset$, where $\{x_a\}$ is the set of periodic points belonging to the cycle a. Thus $\mathbf{C}$ generates a second orbit with the same number of points and the same stability properties. Both orbits give the same contribution to the first term and no contribution to the second term in (22.1); as they are degenerate, the prefactor 1/2 cancels. Resuming as in the derivation of (15.15) we find

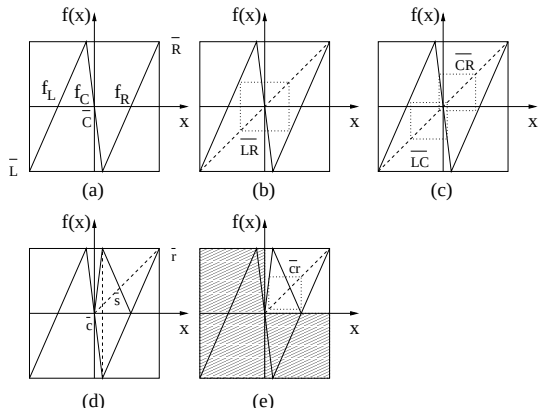

Figure 22.1: The Ulam sawtooth map with the C_2 symmetry $f(-x) = -f(x)$. (a) boundary fixed point $\overline{C}$, (b) symmetric 2-cycle $\overline{LR}$, (c) asymmetric 2-cycles pair $\{\overline{LC},\overline{CR}\}$. The Ulam sawtooth map restricted to the fundamental domain; pieces of the global map (a) are reflected into the upper right quadrant. (d) Boundary fixed point $\overline{C}$ maps into the fixed point $\overline{c}$, symmetric 2-cycle $\overline{LR}$ maps into fixed point $\overline{s}$, and the asymmetric fixed point pair $\{\overline{L},\overline{R}\}$ maps into a single fixed point $\overline{r}$, (e) the asymmetric 2-cycles pair $\{\overline{LC},\overline{CR}\}$ maps into a single 2-cycle $\overline{cr}$.

that asymmetric orbits yield the same contribution to the symmetric and the antisymmetric subspaces:

$$\det(1-\mathcal{L}_\pm)_a = \prod_a \prod_{k=0}^{\infty}\left(1-\frac{t_a}{\Lambda_a^k}\right)\,, \quad t_a = \frac{z^{n_a}}{|\Lambda_a|}\,.$$

Symmetric cycles: A cycle s is reflection symmetric if operating with $\mathbf{C}$ on the set of cycle points reproduces the set. The period of a symmetric cycle is always even ($n_s = 2n_{\tilde{s}}$) and the mirror image of the x_s cycle point is reached by traversing the irreducible segment $\tilde{s}$ of length $n_{\tilde{s}}$, $f^{n_{\tilde{s}}}(x_s) = \mathbf{C}x_s$. $\delta(x-f^n(x))$ picks up $2n_{\tilde{s}}$ contributions for every even traversal, $n = rn_{\tilde{s}}$, r even, and $\delta(x+f^n(x))$ for every odd traversal, $n = rn_{\tilde{s}}$, r odd. Absorb the group-theoretic prefactor in the stability eigenvalue by defining the stability computed for a segment of length $n_{\tilde{s}}$,

$$\Lambda_{\tilde{s}} = -\left.\frac{\partial f^{n_{\tilde{s}}}(x)}{\partial x}\right|_{x=x_s}\,.$$

Restricting the integration to the infinitesimal neighborhood $\mathcal{M}_s$ of the s cycle, we obtain the contribution to $\mathrm{tr}\,\mathcal{L}_\pm^n$:

$$z^n \mathrm{tr}\,\mathcal{L}_\pm^n \;\to\; \int_{\mathcal{M}_s} dx\, z^n\, \frac{1}{2}\left(\delta(x-f^n(x)) \pm \delta(x+f^n(x))\right)$$

$$
\begin{aligned}
&= n_{\bar{s}}\left(\sum_{r=2}^{\text{even}}\delta_{n,rn_{\bar{s}}}\frac{t_{\bar{s}}^r}{1-1/\Lambda_{\bar{s}}^r}\pm\sum_{r=1}^{\text{odd}}\delta_{n,rn_{\bar{s}}}\frac{t_{\bar{s}}^r}{1-1/\Lambda_{\bar{s}}^r}\right)\\
&= n_{\bar{s}}\sum_{r=1}^{\infty}\delta_{n,rn_{\bar{s}}}\frac{(\pm t_{\bar{s}})^r}{1-1/\Lambda_{\bar{s}}^r}\,.
\end{aligned}
$$

Substituting all symmetric cycles s into $\det(1-\mathcal{L}_\pm)$ and resuming we obtain:

$$
\det(1-\mathcal{L}_\pm)_{\bar{s}}=\prod_{\bar{s}}\prod_{k=0}^{\infty}\left(1\mp\frac{t_{\bar{s}}}{\Lambda_{\bar{s}}^k}\right)
$$

Boundary cycles: In the example at hand there is only one cycle which is neither symmetric nor antisymmetric, but lies on the boundary of the fundamental domain, the fixed point at the origin. Such cycle contributes simultaneously to both $\delta(x-f^n(x))$ and $\delta(x+f^n(x))$:

$$
\begin{aligned}
z^n\mathrm{tr}\,\mathcal{L}_\pm^n &\to \int_{\mathcal{M}_b}dx\,z^n\,\frac{1}{2}\left(\delta(x-f^n(x))\pm\delta(x+f^n(x))\right)\\
&= \sum_{r=1}^{\infty}\delta_{n,r}\,t_b^r\,\frac{1}{2}\left(\frac{1}{1-1/\Lambda_b^r}\pm\frac{1}{1+1/\Lambda_b^r}\right)\\
z^n\,\mathrm{tr}\,\mathcal{L}_+^n &\to \sum_{r=1}^{\infty}\delta_{n,r}\frac{t_b^r}{1-1/\Lambda_b^{2r}}\,;\qquad z^n\,\mathrm{tr}\,\mathcal{L}_-^n\to\sum_{r=1}^{\infty}\delta_{n,r}\frac{1}{\Lambda_b^r}\frac{t_b^r}{1-1/\Lambda_b^{2r}}\,.
\end{aligned}
$$

Boundary orbit contributions to the factorized spectral determinants follow by resummation:

$$
\det(1-\mathcal{L}_+)_b=\prod_{k=0}^{\infty}\left(1-\frac{t_b}{\Lambda_b^{2k}}\right)\,,\qquad \det(1-\mathcal{L}_-)_b=\prod_{k=0}^{\infty}\left(1-\frac{t_b}{\Lambda_b^{2k+1}}\right)
$$

Only even derivatives contribute to the symmetric subspace (and odd to the antisymmetric subspace) because the orbit lies on the boundary.

Finally, the symmetry reduced spectral determinants follow by collecting the above results:

$$
F_+(z)=\prod_a\prod_{k=0}^{\infty}\left(1-\frac{t_a}{\Lambda_a^k}\right)\prod_{\bar{s}}\prod_{k=0}^{\infty}\left(1-\frac{t_{\bar{s}}}{\Lambda_{\bar{s}}^k}\right)\prod_{k=0}^{\infty}\left(1-\frac{t_b}{\Lambda_b^{2k}}\right)
$$

$$
F_-(z)=\prod_a\prod_{k=0}^{\infty}\left(1-\frac{t_a}{\Lambda_a^k}\right)\prod_{\bar{s}}\prod_{k=0}^{\infty}\left(1+\frac{t_{\bar{s}}}{\Lambda_{\bar{s}}^k}\right)\prod_{k=0}^{\infty}\left(1-\frac{t_b}{\Lambda_b^{2k+1}}\right) \quad (22.2)
$$

We shall work out the symbolic dynamics of such reflection symmetric systems in some detail in sect. 22.5. As reflection symmetry is essentially the only discrete symmetry that a map of the interval can have, this example completes the group-theoretic factorization of determinants and zeta functions for 1-d maps. We now turn to discussion of the general case.

22.1
page 410

22.2 Discrete symmetries

A dynamical system is invariant under a symmetry group $G=\{e,g_2,\ldots,g_{|G|}\}$ if the equations of motion are invariant under all symmetries $g\in G$. For a map $x_{n+1}=f(x_n)$ and the evolution operator $\mathcal{L}(y,x)$ defined by (10.23) this means

$$
\begin{aligned}
f(x) &= \mathbf{g}^{-1}f(\mathbf{g}x)\\
\mathcal{L}(y,x) &= \mathcal{L}(\mathbf{g}y,\mathbf{g}x)\,.
\end{aligned}
\qquad (22.3)
$$

Bold face letters for group elements indicate a suitable representation on state space. For example, if a 2-dimensional map has the symmetry $x_1\to -x_1$, $x_2\to -x_2$, the symmetry group G consists of the identity and C, a rotation by π around the origin. The map f must then commute with rotations by π, $f(\mathbf{C}x)=\mathbf{C}f(x)$, with $\mathbf{C}$ given by the $[2\times 2]$ matrix

$$
\mathbf{C}=\begin{pmatrix}-1 & 0\\ 0 & -1\end{pmatrix}\,. \qquad (22.4)
$$

$\mathbf{C}$ satisfies $\mathbf{C}^2=e$ and can be used to decompose the state space into mutually orthogonal symmetric and antisymmetric subspaces by means of projection operators (22.1). More generally the projection operator onto the α irreducible subspace of dimension d_α is given by $P_\alpha=(d_\alpha/|G|)\sum\chi_\alpha(h)\mathbf{h}^{-1}$, where $\chi_\alpha(h)=\mathrm{tr}\,D_\alpha(h)$ are the group characters, and the transfer operator $\mathcal{L}$ splits into a sum of inequivalent irreducible subspace contributions $\sum_\alpha\mathrm{tr}\,\mathcal{L}_\alpha$,

$$
\mathcal{L}_\alpha(y,x)=\frac{d_\alpha}{|G|}\sum_{h\in G}\chi_\alpha(h)\mathcal{L}(\mathbf{h}^{-1}y,x)\,. \qquad (22.5)
$$

The prefactor d_α in the above reflects the fact that a d_α-dimensional representation occurs d_α times.

22.2.1 Cycle degeneracies

If $g\in G$ is a symmetry of the dynamical problem, the weight of a cycle p and the weight of its image under a symmetry transformation g are equal,

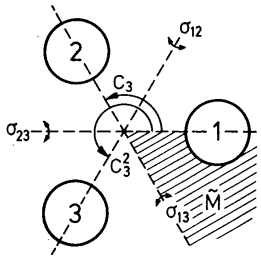

Figure 22.2: The symmetries of three disks on an equilateral triangle. The fundamental domain is indicated by the shaded wedge.

$t_{gp} = t_p$. The number of degenerate cycles (topologically distinct, but mapped into each other by symmetry transformations) depends on the cycle symmetries. Associated with a given cycle p is a maximal subgroup $\mathcal{H}_p \subseteq G$, $\mathcal{H}_p = \{e, b_2, b_3, \ldots, b_h\}$ of order h_p, whose elements leave p invariant. The elements of the quotient space $b \in G/\mathcal{H}_p$ generate the degenerate cycles bp, so the multiplicity of a degenerate cycle is $m_p = g/h_p$.

Taking into account these degeneracies, the Euler product (15.15) takes the form

$$\prod_p (1 - t_p) = \prod_{\hat{p}} (1 - t_{\hat{p}})^{m_{\hat{p}}}. \tag{22.6}$$

Here $\hat{p}$ is one of the m_p degenerate cycles, picked to serve as the label for the entire class. Our labeling convention is usually lexical, i.e., we label a cycle p by the cycle point whose label has the lowest value, and we label a class of degenerate cycles by the one with the lowest label $\hat{p}$. In what follows we shall drop the hat in $\hat{p}$ when it is clear from the context that we are dealing with symmetry distinct classes of cycles.

22.2.2 Example: C_{3v} invariance

An illustration of the above is afforded by C_{3v}, the group of symmetries of a game of pinball with three equal size, equally spaced disks, figure 22.2. The group consists of the identity element e, three reflections across axes $\{\sigma_{12}, \sigma_{23}, \sigma_{13}\}$, and two rotations by $2\pi/3$ and $4\pi/3$ denoted $\{C_3, C_3^2\}$, so its dimension is $g = 6$. On the disk labels $\{1, 2, 3\}$ these symmetries act as permutations which map cycles into cycles. For example, the flip across the symmetry axis going through disk 1 interchanges the symbols 2 and 3; it maps the cycle $\overline{12123}$ into $\overline{13132}$, figure 22.3a.

The subgroups of C_{3v} are C_v, consisting of the identity and any one of the reflections, of dimension $h = 2$, and $C_3 = \{e, C_3, C_3^2\}$, of dimension $h = 3$, so possible cycle multiplicities are $g/h = 2$, 3 or 6.

The C_3 subgroup invariance is exemplified by the cycles $\overline{123}$ and $\overline{132}$ which are invariant under rotations by $2\pi/3$ and $4\pi/3$, but are mapped

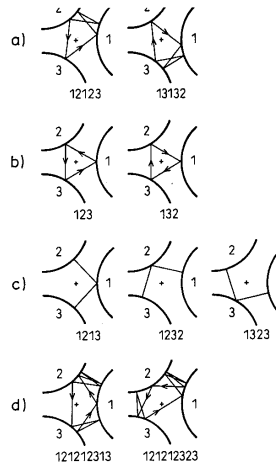

Figure 22.3: Some examples of 3-disk cycles: (a) $\overline{12123}$ and $\overline{13132}$ are mapped into each other by σ_{23}, the flip across 1 axis; this cycle has degeneracy 6 under C_{3v} symmetries. (C_{3v} is the symmetry group of the equilateral triangle.) Similarly (b) $\overline{123}$ and $\overline{132}$ and (c) $\overline{1213}$, $\overline{1232}$ and $\overline{1323}$ are degenerate under C_{3v}. (d) The cycles $\overline{121212313}$ and $\overline{121212323}$ are related by time reversal but not by any C_{3v} symmetry. (from ref. [1.6])

into each other by any reflection, figure 22.3b; $\mathcal{H}_p = \{e, C_3, C_3^2\}$, and the degeneracy is $g/h_{c_3} = 2$.

The C_v type of a subgroup is exemplified by the invariances of $\hat{p} = 1213$. This cycle is invariant under reflection $\sigma_{23}\{\overline{1213}\} = \overline{1312} = \overline{1213}$, so the invariant subgroup is $\mathcal{H}_{\hat{p}} = \{e, \sigma_{23}\}$. Its order is $h_{C_v} = 2$, so the degeneracy is $m_{\hat{p}} = g/h_{C_v} = 3$; the cycles in this class, $\overline{1213}$, $\overline{1232}$ and $\overline{1323}$, are related by $2\pi/3$ rotations, figure 22.3(c).

A cycle of no symmetry, such as $\overline{12123}$, has $\mathcal{H}_p = \{e\}$ and contributes in all six terms (the remaining cycles in the class are $\overline{12132}$, $\overline{12313}$, $\overline{12323}$, $\overline{13132}$ and $\overline{13232}$), figure 22.3a.

Besides the above discrete symmetries, for Hamiltonian systems cycles may be related by time reversal symmetry. An example are the cycles $\overline{121212313}$ and $\overline{121212323} = \overline{313212121}$ which are related by no space symmetry (figure 22.3(d)).

The Euler product (15.15) for the C_{3v} symmetric 3-disk problem is given in (18.33).

22.3 Dynamics in the fundamental domain

So far we have used the discrete symmetry to effect a reduction in the number of independent cycles in cycle expansions. The next step achieves much more: the symmetries can be used to restrict all computations to a *fundamental domain*. We show here that to each global cycle p corresponds a fundamental domain cycle $\tilde{p}$. Conversely, each fundamental domain cycle

$\tilde{p}$ traces out a segment of the global cycle p, with the end point of the cycle $\tilde{p}$ mapped into the irreducible segment of p with the group element $h_{\tilde{p}}$.

An important effect of a discrete symmetry is that it tessellates the state space into copies of a fundamental domain, and thus induces a natural partition of phase space. The group elements $g = \{a, b, \cdots, d\}$ which map the fundamental domain $\tilde{M}$ into its copies $g\tilde{M}$, can double in function as letters of a symbolic dynamics alphabet. If the dynamics is symmetric under interchanges of disks, the absolute disk labels $\epsilon_i = 1, 2, \cdots, N$ can be replaced by the symmetry-invariant relative disk→disk increments g_i, where g_i is the discrete group element that maps disk $i-1$ into disk i. We demonstrate the reduction for a series of specific examples in sect. 22.4. An immediate gain arising from symmetry invariant relabeling is that N-disk symbolic dynamics becomes $(N-1)$-nary, with no restrictions on the admissible sequences. However, the main gain is in the close connection between the symbol string symmetries and the state space symmetries which will aid us in the dynamical zeta function factorizations. Once the connection between the full space and the reduced space is established, working in the fundamental domain (*ie.*, with irreducible segments) is so much simpler that we never use the full space orbits in actual computations.

If the dynamics is invariant under a discrete symmetry, the state space M can be completely tiled by the fundamental domain $\tilde{M}$ and its images $a\tilde{M}$, $b\tilde{M}$, ... under the action of the symmetry group $G = \{e, a, b, \ldots\}$,

$$M = \sum_{a \in G} M_a = \sum_{a \in G} a\tilde{M} \, .$$

In the above example (22.4) with symmetry group $G = \{e, C\}$, the state space $M = \{x_1\text{-}x_2 \text{ plane}\}$ can be tiled by a fundamental domain $\tilde{M} = \{\text{half-plane } x_1 \geq 0\}$, and $\mathbf{C}\tilde{M} = \{\text{half-plane } x_1 \leq 0\}$, its image under rotation by π.

If the space M is decomposed into g tiles, a function $\phi(x)$ over M splits into a g-dimensional vector $\phi_a(x)$ defined by $\phi_a(x) = \phi(x)$ if $x \in M_a$, $\phi_a(x) = 0$ otherwise. Let $h = ab^{-1}$ conflicts with be the symmetry operation that maps the endpoint domain M_b into the starting point domain M_a, and let $D(h)_{ba}$, the left regular representation, be the $[g \times g]$ matrix whose b, a-th entry equals unity if $a = hb$ and zero otherwise; $D(h)_{ba} = \delta_{bh,a}$. Since the symmetries act on state space as well, the operation h enters in two guises: as a $[g \times g]$ matrix $D(h)$ which simply permutes the domain labels, and as a $[d \times d]$ matrix representation $\mathbf{h}$ of a discrete symmetry operation on the d state space coordinates. For instance, in the above example (22.4) $h \in C_2$ and $D(h)$ can be either the identity or the interchange of the two domain labels,

$$D(e) = \begin{pmatrix} 1 & 0 \\ 0 & 1 \end{pmatrix} \, , \quad D(C) = \begin{pmatrix} 0 & 1 \\ 1 & 0 \end{pmatrix} \, . \tag{22.7}$$

Note that $D(h)$ is a permutation matrix, mapping a tile M_a into a different tile $M_{ha} \neq M_a$ if $h \neq e$. Consequently only $D(e)$ has diagonal elements, and $\mathrm{tr}\, D(h) = g\delta_{h,e}$. However, the state space transformation $\mathbf{h} \neq \mathbf{e}$ leaves invariant sets of *boundary* points; for example, under reflection σ across a symmetry axis, the axis itself remains invariant. The boundary periodic orbits that belong to such point-wise invariant sets will require special care in $\mathrm{tr}\, \mathcal{L}$ evaluations.

One can associate to the evolution operator (10.23) a $[g \times g]$ matrix evolution operator defined by

$$\mathcal{L}_{ba}(y, x) = D(h)_{ba} \mathcal{L}(y, x) \, ,$$

if $x \in M_a$ and $y \in M_b$, and zero otherwise. Now we can use the invariance condition (22.3) to move the starting point x into the fundamental domain $x = \mathbf{a}\tilde{x}$, $\mathcal{L}(y, x) = \mathcal{L}(\mathbf{a}^{-1}y, \tilde{x})$, and then use the relation $a^{-1}b = h^{-1}$ to also relate the endpoint y to its image in the fundamental domain, $\tilde{\mathcal{L}}(\tilde{y}, \tilde{x}) := \mathcal{L}(\mathbf{h}^{-1}\tilde{y}, \tilde{x})$. With this operator which is restricted to the fundamental domain, the global dynamics reduces to

$$\mathcal{L}_{ba}(y, x) = D(h)_{ba} \tilde{\mathcal{L}}(\tilde{y}, \tilde{x}) \, .$$

While the global trajectory runs over the full space M, the restricted trajectory is brought back into the fundamental domain $\tilde{M}$ any time it crosses into adjoining tiles; the two trajectories are related by the symmetry operation h which maps the global endpoint into its fundamental domain image.

Now the traces (15.3) required for the evaluation of the eigenvalues of the transfer operator can be evaluated on the fundamental domain alone

$$\mathrm{tr}\, \mathcal{L} = \int_M dx \mathcal{L}(x, x) = \int_{\tilde{M}} d\tilde{x} \, \sum_h \mathrm{tr}\, D(h) \; \mathcal{L}(\mathbf{h}^{-1}\tilde{x}, \tilde{x}) \tag{22.8}$$

The fundamental domain integral $\int d\tilde{x} \; \mathcal{L}(\mathbf{h}^{-1}\tilde{x}, \tilde{x})$ picks up a contribution from every global cycle (for which $h = e$), but it also picks up contributions from shorter segments of global cycles. The permutation matrix $D(h)$ guarantees by the identity $\mathrm{tr}\, D(h) = 0$, $h \neq e$, that only those repeats of the fundamental domain cycles $\tilde{p}$ that correspond to complete global cycles p contribute. Compare, for example, the contributions of the $\overline{12}$ and $\overline{0}$ cycles of figure 11.6. $\mathrm{tr}\, D(h)\tilde{\mathcal{L}}$ does not get a contribution from the $\overline{0}$ cycle, as the symmetry operation that maps the first half of the $\overline{12}$ into the fundamental domain is a reflection, and $\mathrm{tr}\, D(\sigma) = 0$. In contrast, $\sigma^2 = e$, $\mathrm{tr}\, D(\sigma^2) = 6$ insures that the repeat of the fundamental domain fixed point $\mathrm{tr}\, (D(h)\tilde{\mathcal{L}})^2 = 6t_0^2$, gives the correct contribution to the global trace $\mathrm{tr}\, \mathcal{L}^2 = 3 \cdot 2t_{12}$.

Let p be the full orbit, $\tilde{p}$ the orbit in the fundamental domain and $h_{\tilde{p}}$ an element of $\mathcal{H}_p$, the symmetry group of p. Restricting the volume integrations to the infinitesimal neighborhoods of the cycles p and $\tilde{p}$, respectively, and performing the standard resummations, we obtain the identity

$$(1-t_p)^{m_p} = \det\,(1-D(h_{\tilde{p}})t_{\tilde{p}})\ , \tag{22.9}$$

valid cycle by cycle in the Euler products (15.15) for $\det(1-\mathcal{L})$. Here "det" refers to the $[g\times g]$ matrix representation $D(h_{\tilde{p}})$; as we shall see, this determinant can be evaluated in terms of standard characters, and no explicit representation of $D(h_{\tilde{p}})$ is needed. Finally, if a cycle p is invariant under the symmetry subgroup $\mathcal{H}_p \subseteq G$ of order h_p, its weight can be written as a repetition of a fundamental domain cycle

$$t_p = t_{\tilde{p}}^{h_p} \tag{22.10}$$

computed on the irreducible segment that corresponds to a fundamental domain cycle. For example, in figure 11.6 we see by inspection that $t_{12} = t_0^2$ and $t_{123} = t_1^3$.

22.3.1 Boundary orbits

Before we can turn to a presentation of the factorizations of dynamical zeta functions for the different symmetries we have to discuss an effect that arises for orbits that run on a symmetry line that borders a fundamental domain. In our 3-disk example, no such orbits are possible, but they exist in other systems, such as in the bounded region of the Hénon-Heiles potential and in 1-d maps. For the symmetrical 4-disk billiard, there are in principle two kinds of such orbits, one kind bouncing back and forth between two diagonally opposed disks and the other kind moving along the other axis of reflection symmetry; the latter exists for bounded systems only. While there are typically very few boundary orbits, they tend to be among the shortest orbits, and their neglect can seriously degrade the convergence of cycle expansions, as those are dominated by the shortest cycles.

While such orbits are invariant under some symmetry operations, their neighborhoods are not. This affects the stability matrix M_p of the linearization perpendicular to the orbit and thus the eigenvalues. Typically, *e.g.* if the symmetry is a reflection, some eigenvalues of M_p change sign. This means that instead of a weight $1/\det(\mathbf{1}-M_p)$ as for a regular orbit, boundary cycles also pick up contributions of form $1/\det(\mathbf{1}-\mathbf{h}M_p)$, where $\mathbf{h}$ is a symmetry operation that leaves the orbit pointwise invariant; see for example sect. 22.1.2.

Consequences for the dynamical zeta function factorizations are that sometimes a boundary orbit does not contribute. A derivation of a dynamical zeta function (15.15) from a determinant like (15.9) usually starts

with an expansion of the determinants of the Jacobian. The leading order terms just contain the product of the expanding eigenvalues and lead to the dynamical zeta function (15.15). Next to leading order terms contain products of expanding and contracting eigenvalues and are sensitive to their signs. Clearly, the weights t_p in the dynamical zeta function will then be affected by reflections in the Poincaré surface of section perpendicular to the orbit. In all our applications it was possible to implement these effects by the following simple prescription.

If an orbit is invariant under a little group $\mathcal{H}_p = \{e, b_2, \ldots, b_h\}$, then the corresponding group element in (22.9) will be replaced by a projector. If the weights are insensitive to the signs of the eigenvalues, then this projector is

$$g_p = \frac{1}{h}\sum_{i=1}^{h} b_i\,. \tag{22.11}$$

In the cases that we have considered, the change of sign may be taken into account by defining a sign function $\epsilon_p(g) = \pm 1$, with the "-" sign if the symmetry element g flips the neighborhood. Then (22.11) is replaced by

$$g_p = \frac{1}{h}\sum_{i=1}^{h} \epsilon(b_i)\, b_i\,. \tag{22.12}$$

We have illustrated the above in sect. 22.1.2 by working out the full factorization for the 1-dimensional reflection symmetric maps.

22.4 Factorizations of dynamical zeta functions

In the above we have shown that a discrete symmetry induces degeneracies among periodic orbits and decomposes periodic orbits into repetitions of irreducible segments; this reduction to a fundamental domain furthermore leads to a convenient symbolic dynamics compatible with the symmetry, and, most importantly, to a factorization of dynamical zeta functions. This we now develop, first in a general setting and then for specific examples.

22.4.1 Factorizations of dynamical dynamical zeta functions

According to (22.9) and (22.10), the contribution of a degenerate class of global cycles (cycle p with multiplicity $m_p = g/h_p$) to a dynamical zeta function is given by the corresponding fundamental domain cycle $\tilde{p}$:

$$(1-t_{\tilde{p}}^{h_p})^{g/h_p} = \det\,(1-D(h_{\tilde{p}})t_{\tilde{p}}) \tag{22.13}$$

Let $D(h) = \bigoplus_\alpha d_\alpha D_\alpha(h)$ be the decomposition of the matrix representation $D(h)$ into the d_α dimensional irreducible representations α of a finite group G. Such decompositions are block-diagonal, so the corresponding contribution to the Euler product (15.9) factorizes as

$$\det(1 - D(h)t) = \prod_\alpha \det(1 - D_\alpha(h)t)^{d_\alpha} , \tag{22.14}$$

where now the product extends over all distinct d_α-dimensional irreducible representations, each contributing d_α times. For the cycle expansion purposes, it has been convenient to emphasize that the group-theoretic factorization can be effected cycle by cycle, as in (22.13); but from the transfer operator point of view, the key observation is that the symmetry reduces the transfer operator to a block diagonal form; this block diagonalization implies that the dynamical zeta functions (15.15) factorize as

$$\frac{1}{\zeta} = \prod_\alpha \frac{1}{\zeta_\alpha^{d_\alpha}} , \qquad \frac{1}{\zeta_\alpha} = \prod_{\tilde p} \det\,(1 - D_\alpha(h_{\tilde p})t_{\tilde p}) \ . \tag{22.15}$$

Determinants of d-dimensional irreducible representations can be evaluated using the expansion of determinants in terms of traces,

$$\begin{aligned}\det(1+M) &= 1 + \operatorname{tr} M + \frac{1}{2}\left((\operatorname{tr} M)^2 - \operatorname{tr} M^2\right) \\ &\quad + \frac{1}{6}\left((\operatorname{tr} M)^3 - 3(\operatorname{tr} M)(\operatorname{tr} M^2) + 2\operatorname{tr} M^3\right) \\ &\quad + \cdots + \frac{1}{d!}\left((\operatorname{tr} M)^d - \cdots\right) ,\end{aligned} \tag{22.16}$$

(see (J.26), for example) and each factor in (22.14) can be evaluated by looking up the characters $\chi_\alpha(h) = \operatorname{tr} D_\alpha(h)$ in standard tables [22.15]. In terms of characters, we have for the 1-dimensional representations

$$\det(1 - D_\alpha(h)t) = 1 - \chi_\alpha(h)t ,$$

for the 2-dimensional representations

$$\det(1 - D_\alpha(h)t) = 1 - \chi_\alpha(h)t + \frac{1}{2}\left(\chi_\alpha(h)^2 - \chi_\alpha(h^2)\right)t^2,$$

and so forth.

In the fully symmetric subspace $\operatorname{tr} D_{A_1}(h) = 1$ for all orbits; hence a straightforward fundamental domain computation (with no group theory weights) always yields a part of the full spectrum. In practice this is the most interesting subspectrum, as it contains the leading eigenvalue of the transfer operator.

22.2
page 410

22.4.2 Factorizations of spectral determinants

Factorization of the full spectral determinant (15.3) proceeds in essentially the same manner as the factorization of dynamical zeta functions outlined above. By (22.5) and (22.8) the trace of the transfer operator $\mathcal{L}$ splits into the sum of inequivalent irreducible subspace contributions $\sum_\alpha \operatorname{tr}\mathcal{L}_\alpha$, with

$$\operatorname{tr}\mathcal{L}_\alpha = d_\alpha \sum_{h\in G} \chi_\alpha(h) \int_{\tilde M} d\tilde x\, \mathcal{L}(\mathbf{h}^{-1}\tilde x, \tilde x) .$$

This leads by standard manipulations to the factorization of (15.9) into

$$\begin{aligned} F(z) &= \prod_\alpha F_\alpha(z)^{d_\alpha} \\ F_\alpha(z) &= \exp\left(-\sum_{\tilde p}\sum_{r=1}^{\infty}\frac{1}{r}\frac{\chi_\alpha(h_{\tilde p}^r) z^{n_{\tilde p} r}}{|\det\left(\mathbf{1} - \tilde M_{\tilde p}^r\right)|}\right) , \end{aligned} \tag{22.17}$$

where $\tilde M_{\tilde p} = \mathbf{h}_{\tilde p} M_{\tilde p}$ is the fundamental domain Jacobian. Boundary orbits require special treatment, discussed in sect. 22.3.1, with examples given in the next section as well as in the specific factorizations discussed below.

The factorizations (22.15), (22.17) are the central formulas of this chapter. We now work out the group theory factorizations of cycle expansions of dynamical zeta functions for the cases of C_2 and C_{3v} symmetries. The cases of the C_{2v}, C_{4v} symmetries are worked out in appendix H below.

22.5
page 411

22.5 C_2 factorization

As the simplest example of implementing the above scheme consider the C_2 symmetry. For our purposes, all that we need to know here is that each orbit or configuration is uniquely labeled by an infinite string $\{s_i\}$, $s_i = +, -$ and that the dynamics is invariant under the $+ \leftrightarrow -$ interchange, i.e., it is C_2 symmetric. The C_2 symmetry cycles separate into two classes, the self-dual configurations $+-$, $++--$, $+++---$, $+--+-++-$, $\cdots$, with multiplicity $m_p = 1$, and the asymmetric configurations $+$, $-$, $++-$, $--+$, $\cdots$, with multiplicity $m_p = 2$. For example, as there is no absolute distinction between the "up" and the "down" spins, or the "left" or the "right" lobe, $t_+ = t_-$, $t_{++-} = t_{+--}$, and so on.

The symmetry reduced labeling $\rho_i \in \{0, 1\}$ is related to the standard $s_i \in \{+, -\}$ Ising spin labeling by

$$\begin{aligned} &\text{If} \quad s_i = s_{i-1} \quad \text{then} \quad \rho_i = 1 \\ &\text{If} \quad s_i \neq s_{i-1} \quad \text{then} \quad \rho_i = 0 \end{aligned} \tag{22.18}$$

$\tilde{p}$	p	m_p
1	$+$	2
0	$-+$	1
01	$--\ ++$	1
001	$-++$	2
011	$---\ +++$	1
0001	$-+--\ +-++$	1
0011	$-+++$	2
0111	$----\ ++++$	1
00001	$-+-+-$	2
00011	$-+----\ +-+++$	1
00101	$-++--\ +--++$	1
00111	$-+---\ +-+++$	1
01011	$--+++$	2
01111	$-----\ +++++$	1
001011	$-++---\ +--+++$	1
001101	$-+++--\ +---++$	1

Table 22.1: Correspondence between the C_2 symmetry reduced cycles $\tilde{p}$ and the standard Ising model periodic configurations p, together with their multiplicities m_p. Also listed are the two shortest cycles (length 6) related by time reversal, but distinct under C_2.

For example, $\overline{+} = \cdots+++\cdots$ maps into $\cdots111\cdots = \overline{1}$ (and so does $\overline{-}$), $\overline{-+} = \cdots-+-+\cdots$ maps into $\cdots000\cdots = \overline{0}$, $\overline{-++-} = \cdots--++--+$ $+\cdots$ maps into $\cdots0101\cdots = \overline{01}$, and so forth. A list of such reductions is given in table 22.1.

Depending on the maximal symmetry group $\mathcal{H}_p$ that leaves an orbit p invariant (see sects. 22.2 and 22.3 as well as sect. 22.1.2), the contributions to the dynamical zeta function factor as

$$\begin{array}{rrcl} & & A_1 & A_2 \\ \mathcal{H}_p = \{e\}: & (1-t_{\tilde{p}})^2 & = & (1-t_{\tilde{p}})(1-t_{\tilde{p}}) \\ \mathcal{H}_p = \{e,\sigma\}: & (1-t_{\tilde{p}}^2) & = & (1-t_{\tilde{p}})(1+t_{\tilde{p}})\ , \end{array} \tag{22.19}$$

For example:

$$\begin{aligned} \mathcal{H}_{++-} = \{e\}: &\quad (1-t_{++-})^2 &&= (1-t_{001})(1-t_{001}) \\ \mathcal{H}_{+-} = \{e,\sigma\}: &\quad (1-t_{+-}) &&= (1-t_0)\ (1+t_0), \quad t_{+-} = t_0^2 \end{aligned}$$

This yields two binary cycle expansions. The A_1 subspace dynamical zeta function is given by the standard binary expansion (18.5). The antisymmetric A_2 subspace dynamical zeta function ζ_{A_2} differs from ζ_{A_1} only by a minus sign for cycles with an odd number of 0's:

$$\begin{aligned} 1/\zeta_{A_2} &= (1+t_0)(1-t_1)(1+t_{10})(1-t_{100})(1+t_{101})(1+t_{1000}) \\ &\quad (1-t_{1001})(1+t_{1011})(1-t_{10000})(1+t_{10001}) \\ &\quad (1+t_{10010})(1-t_{10011})(1-t_{10101})(1+t_{10111})\ldots \\ &= 1+t_0-t_1+(t_{10}-t_1t_0)-(t_{100}-t_{10}t_0)+(t_{101}-t_{10}t_1) \\ &\quad -(t_{1001}-t_1t_{001}-t_{101}t_0+t_{10}t_0t_1)-\ldots\ldots \end{aligned} \tag{22.20}$$

Note that the group theory factors do not destroy the curvature corrections (the cycles and pseudo cycles are still arranged into shadowing combinations).

If the system under consideration has a boundary orbit (*cf.* sect. 22.3.1) with group-theoretic factor $\mathbf{h}_p = (\mathbf{e}+\sigma)/2$, the boundary orbit does not contribute to the antisymmetric subspace

$$\begin{array}{rrcl} & & A_1 & A_2 \\ \text{boundary:} & (1-t_p) & = & (1-t_{\tilde{p}})(1-0t_{\tilde{p}}) \end{array} \tag{22.21}$$

This is the $1/\zeta$ part of the boundary orbit factorization of sect. 22.1.2.

22.6 C_{3v} factorization: 3-disk game of pinball

The next example, the C_{3v} symmetry, can be worked out by a glance at figure 11.6a. For the symmetric 3-disk game of pinball the fundamental domain is bounded by a disk segment and the two adjacent sections of the symmetry axes that act as mirrors (see figure 11.6b). The three symmetry axes divide the space into six copies of the fundamental domain. Any trajectory on the full space can be pieced together from bounces in the fundamental domain, with symmetry axes replaced by flat mirror reflections. The binary $\{0,1\}$ reduction of the ternary three disk $\{1,2,3\}$ labels has a simple geometric interpretation: a collision of type 0 reflects the projectile to the disk it comes from (back–scatter), whereas after a collision of type 1 projectile continues to the third disk. For example, $\overline{23} = \cdots232323\cdots$ maps into $\cdots000\cdots = \overline{0}$ (and so do $\overline{12}$ and $\overline{13}$), $\overline{123} = \cdots12312\cdots$ maps into $\cdots111\cdots = \overline{1}$ (and so does $\overline{132}$), and so forth. A list of such reductions for short cycles is given in table 11.2.

C_{3v} has two 1-dimensional irreducible representations, symmetric and antisymmetric under reflections, denoted A_1 and A_2, and a pair of degenerate 2-dimensional representations of mixed symmetry, denoted E. The contribution of an orbit with symmetry g to the $1/\zeta$ Euler product (22.14) factorizes according to

$$\det(1-D(h)t) = (1-\chi_{A_1}(h)t)\,(1-\chi_{A_2}(h)t)\left(1-\chi_E(h)t+\chi_{A_2}(h)t^2\right)^2 \tag{22.22}$$

with the three factors contributing to the C_{3v} irreducible representations A_1, A_2 and E, respectively, and the 3-disk dynamical zeta function factorizes into $\zeta = \zeta_{A_1}\zeta_{A_2}\zeta_E^2$. Substituting the C_{3v} characters [22.15]

C_{3v}	A_1	A_2	E
e	1	1	2
C_3, C_3^2	1	1	-1
σ_v	1	-1	0

into (22.22), we obtain for the three classes of possible orbit symmetries (indicated in the first column)

$$\begin{array}{rrcl} & \mathbf{h}_{\tilde{p}} & & A_1 \quad A_2 \quad E \\ e: & (1-t_{\tilde{p}})^6 & = & (1-t_{\tilde{p}})(1-t_{\tilde{p}})(1-2t_{\tilde{p}}+t_{\tilde{p}}^2)^2 \\ C_3, C_3^2: & (1-t_{\tilde{p}}^3)^2 & = & (1-t_{\tilde{p}})(1-t_{\tilde{p}})(1+\ t_{\tilde{p}}+t_{\tilde{p}}^2)^2 \\ \sigma_v: & (1-t_{\tilde{p}}^2)^3 & = & (1-t_{\tilde{p}})(1+t_{\tilde{p}})(1+0t_{\tilde{p}}-t_{\tilde{p}}^2)^2. \end{array} \tag{22.23}$$

where σ_v stands for any one of the three reflections.

The Euler product (15.15) on each irreducible subspace follows from the factorization (22.23). On the symmetric A_1 subspace the ζ_{A_1} is given by the standard binary curvature expansion (18.5). The antisymmetric A_2 subspace ζ_{A_2} differs from ζ_{A_1} only by a minus sign for cycles with an odd number of 0's, and is given in (22.20). For the mixed-symmetry subspace E the curvature expansion is given by

$$\begin{aligned} 1/\zeta_E &= (1+zt_1+z^2t_1^2)(1-z^2t_0^2)(1+z^3t_{100}+z^6t_{100}^2)(1-z^4t_{10}^2) \\ &\quad (1+z^4t_{1001}+z^8t_{1001}^2)(1+z^5t_{10000}+z^{10}t_{10000}^2) \\ &\quad (1+z^5t_{10101}+z^{10}t_{10101}^2)(1-z^5t_{10011})^2\dots \\ &= 1+zt_1+z^2(t_1^2-t_0^2)+z^3(t_{001}-t_1t_0^2) \\ &\quad +z^4\left[t_{0011}+(t_{001}-t_1t_0^2)t_1-t_{01}^2\right] \\ &\quad +z^5\left[t_{00001}+t_{01011}-2t_{00111}+(t_{0011}-t_{01}^2)t_1+(t_1^2-t_0^2)t_{100}\right] \end{aligned} \tag{22.24}$$

We have reinserted the powers of z in order to group together cycles and pseudocycles of the same length. Note that the factorized cycle expansions retain the curvature form; long cycles are still shadowed by (somewhat less obvious) combinations of pseudocycles.

Referring back to the topological polynomial (13.31) obtained by setting $t_p = 1$, we see that its factorization is a consequence of the C_{3v} factorization of the ζ function:

$$1/\zeta_{A_1} = 1-2z\ , \quad 1/\zeta_{A_2} = 1\ , \quad 1/\zeta_E = 1+z\ , \tag{22.25}$$

as obtained from (18.5), (22.20) and (22.24) for $t_p = 1$.

Their symmetry is $K = \{\mathbf{e}, \sigma\}$, so according to (22.11), they pick up the group-theoretic factor $\mathbf{h}_p = (\mathbf{e}+\sigma)/2$. If there is no sign change in t_p, then evaluation of $\det\left(1-\frac{\mathbf{e}+\sigma}{2}t_{\tilde{p}}\right)$ yields

$$\begin{array}{rrcl} & & & A_1 \quad A_2 \quad E \\ \text{boundary:} & (1-t_p)^3 & = & (1-t_{\tilde{p}})(1-0t_{\tilde{p}})(1-t_{\tilde{p}})^2\,, \quad t_p = t_{\tilde{p}} \end{array} \tag{22.26}$$

However, if the cycle weight changes sign under reflection, $t_{\sigma\tilde{p}} = -t_{\tilde{p}}$, the boundary orbit does not contribute to the subspace symmetric under reflection across the orbit;

$$\begin{array}{rrcl} & & & A_1 \quad A_2 \quad E \\ \text{boundary:} & (1-t_p)^3 & = & (1-0t_{\tilde{p}})(1-t_{\tilde{p}})(1-t_{\tilde{p}})^2\,, \quad t_p = t_{\tilde{p}} \end{array} \tag{22.27}$$

Commentary

Remark 22.1 Some examples of systems with discrete symmetries. This chapter is based on ref. [22.1]. One has a C_2 symmetry in the Lorenz system [2.1, 22.16], the Ising model, and in the 3-dimensional anisotropic Kepler potential [31.6, 31.19, 31.20], a C_{3v} symmetry in Hénon-Heiles type potentials [22.2, 22.6, 22.7, 22.5], a C_{4v} symmetry in quartic oscillators [22.9, 22.10], in the pure x^2y^2 potential [22.11, 22.12] and in hydrogen in a magnetic field [22.13], and a $C_{2v} = C_2 \times C_2$ symmetry in the stadium billiard [22.4]. A very nice application of the symmetry factorization is carried out in ref. [22.8].

Remark 22.2 Who did it? This chapter is based on long collaborative effort with B. Eckhardt, ref. [22.1]. The group-theoretic factorizations of dynamical zeta functions that we develop here were first introduced and applied in ref. [6.3]. They are closely related to the symmetrizations introduced by Gutzwiller [31.6] in the context of the semiclassical periodic orbit trace formulas, put into more general group-theoretic context by Robbins [22.4], whose exposition, together with Lauritzen's [22.5] treatment of the boundary orbits, has influenced the presentation given here. A related group-theoretic decomposition in context of hyperbolic billiards was utilized in ref. [22.8].

Remark 22.3 Computations The techniques of this chapter have been applied to computations of the 3-disk classical and quantum spectra in refs. [1.6, 33.15], and to a "Zeeman effect" pinball and the x^2y^2 potentials in refs. [22.3, 18.12]. In a larger perspective, the factorizations developed above are special cases of a general approach to exploiting the group-theoretic invariances in spectra computations, such as those used in enumeration of periodic geodesics [22.8, 15.4, 15.14] for hyperbolic billiards [31.4] and Selberg zeta functions [26.2].

Remark 22.4 Other symmetries. In addition to the symmetries exploited here, time reversal symmetry and a variety of other non-trivial discrete symmetries can induce further relations among orbits; we shall point out several of examples of cycle degeneracies under time reversal. We do not know whether such symmetries can be exploited for further improvements of cycle expansions.

Remark 22.5 Cycles and symmetries. We conclude this section with a few comments about the role of symmetries in actual extraction of cycles. In the

example at hand, the N-disk billiard systems, a fundamental domain is a sliver of the N-disk configuration space delineated by a pair of adjoining symmetry axes, with the directions of the momenta indicated by arrows. The flow may further be reduced to a return map on a Poincaré surface of section, on which an appropriate transfer operator may be constructed. While in principle any Poincaré surface of section will do, a natural choice in the present context are crossings of symmetry axes.

In actual numerical integrations only the last crossing of a symmetry line needs to be determined. The cycle is run in global coordinates and the group elements associated with the crossings of symmetry lines are recorded; integration is terminated when the orbit closes in the fundamental domain. Periodic orbits with non-trivial symmetry subgroups are particularly easy to find since their points lie on crossings of symmetry lines.

Remark 22.6 C_2 symmetry The C_2 symmetry arises, for example, in the Lorenz system [22.16], in the 3-dimensional anisotropic Kepler problem [31.6, 31.19, 31.20] or in the cycle expansions treatments of the Ising model [12.65].

Remark 22.7 Hénon-Heiles potential An example of a system with C_{3v} symmetry is provided by the motion of a particle in the Hénon-Heiles potential [22.2]

$$V(r,\theta) = \frac{1}{2}r^2 + \frac{1}{3}r^3\sin(3\theta) \ .$$

Our coding is not directly applicable to this system because of the existence of elliptic islands and because the three orbits that run along the symmetry axis cannot be labeled in our code. However, since these orbits run along the boundary of the fundamental domain, they require the special treatment discussed in sect. 22.3.1.

Résumé

If a dynamical system has a discrete symmetry, the symmetry should be exploited; much is gained, both in understanding of the spectra and ease of their evaluation. Once this is appreciated, it is hard to conceive of a calculation without factorization; it would correspond to quantum mechanical calculations without wave–function symmetrizations.

Reduction to the fundamental domain simplifies symbolic dynamics and eliminates symmetry induced degeneracies. While the resummation of the theory from the trace sums to the cycle expansions does not reduce the exponential growth in number of cycles with the cycle length, in practice only the short orbits are used, and for them the labor saving is dramatic. For example, for the 3-disk game of pinball there are 256 periodic points of length 8, but reduction to the fundamental domain non-degenerate prime cycles reduces the number of the distinct cycles of length 8 to 30.

In addition, cycle expansions of the symmetry reduced dynamical zeta functions converge dramatically faster than the unfactorized dynamical zeta functions. One reason is that the unfactorized dynamical zeta function has many closely spaced zeros and zeros of multiplicity higher than one; since the cycle expansion is a polynomial expansion in topological cycle length, accommodating such behavior requires many terms. The dynamical zeta functions on separate subspaces have more evenly and widely spaced zeros, are smoother, do not have symmetry-induced multiple zeros, and fewer cycle expansion terms (short cycle truncations) suffice to determine them. Furthermore, the cycles in the fundamental domain sample state space more densely than in the full space. For example, for the 3-disk problem, there are 9 distinct (symmetry unrelated) cycles of length 7 or less in full space, corresponding to 47 distinct periodic points. In the fundamental domain, we have 8 (distinct) periodic orbits up to length 4 and thus 22 different periodic points in 1/6-th the state space, i.e., an increase in density by a factor 3 with the same numerical effort.

We emphasize that the symmetry factorization (22.23) of the dynamical zeta functionis *intrinsic* to the classical dynamics, and not a special property of quantal spectra. The factorization is not restricted to the Hamiltonian systems, or only to the configuration space symmetries; for example, the discrete symmetry can be a symmetry of the Hamiltonian phase space [22.4]. In conclusion, the manifold advantages of the symmetry reduced dynamics should thus be obvious; full space cycle expansions, such as those of exercise 18.8, are useful only for cross checking purposes.

References

[22.1] P. Cvitanović and B. Eckhardt, *"Symmetry decomposition of chaotic dynamics"*, *Nonlinearity* **6**, 277 (1993).

[22.2] M. Henón and C. Heiles, *J. Astron.* **69**, 73 (1964).

[22.3] G. Russberg, (in preparation)

[22.4] J.M. Robbins, *"Semiclassical trace formulas in the presence of continuous symmetries"*, *Phys. Rev.* **A 40**, 2128 (1989).

[22.5] B. Lauritzen, Discrete symmetries and the periodic-orbit expansions, *Phys. Rev.* **A 43** 603, (1991).

[22.6] C. Jung and H.J. Scholz, *J. Phys.* **A 20**, 3607 (1987).

[22.7] C. Jung and P. Richter, *J. Phys.* **A 23**, 2847 (1990).

[22.8] N. Balasz and A. Voros, *Phys. Rep.* **143**, 109 (1986).

[22.9] B. Eckhardt, G. Hose and E. Pollak, *Phys. Rev.* **A 39**, 3776 (1989).

[22.10] C. C. Martens, R. L. Waterland, and W. P. Reinhardt, *J. Chem. Phys.* **90**, 2328 (1989).

[22.11] S.G. Matanyan, G.K. Savvidy, and N.G. Ter-Arutyunyan-Savvidy, *Sov. Phys. JETP 53*, 421 (1981).

[22.12] A. Carnegie and I. C. Percival, *J. Phys.* **A 17**, 801 (1984).

[22.13] B. Eckhardt and D. Wintgen, *J. Phys.* **B 23**, 355 (1990).

[22.14] J.M. Robbins, S.C. Creagh and R.G. Littlejohn, *Phys. Rev.* **A39**, 2838 (1989); **A41**, 6052 (1990).

[22.15] M. Hamermesh, *Group Theory and its Application to Physical Problems* (Addison-Wesley, Reading, 1962).

[22.16] G. Ott and G. Eilenberger, private communication.